Tomography of Soil–Water–Root Processes

Proceedings of a symposium sponsored by Division S-1 and S-6 of the Soil Science Society of America in Minneapolis, Minnesota, 4 Nov. 1992.

SSSA Special Publication Number 36

American Society of Agronomy, Inc.
Soil Science Society of America, Inc.
Madison, Wisconsin, USA

1994

7 Gamma Ray Tomography Measurements of Soil Density Variations in Soil Cores[1]

G. O. Brown, M. L. Stone, J. E. Gazin, and S. R. Clinkscales

Oklahoma State University
Stillwater, Oklahoma

ABSTRACT

Small scale density variations in soil cores were measured and quantified using a gamma ray tomography scanner. The dry bulk density distribution was measured on samples of Norge silty loam (fine-silty, mixed, thermic Udic Paleustoll). The samples differed in size and sampling method. With these measurements the natural density variation within the samples and the effects of sample collection were defined on the scale of 5 mm^3. Driven, 50.8-mm cores were adequate to describe the density variations of the soil matrix. None of the samples were considered adequate to define the soil macropores. The mean density distribution was found to vary over small vertical distances. All samples had density distributions with negative skew and kurtosis less than three. The standard deviation and kurtosis of the density distribution was found to increase with increasing numbers of macropores.

Computerized tomography (CT) is being utilized in soil physics research at an increasing pace. Notable applications include Petrovic et al. (1982), Hainsworth and Aylmore (1983), Crestana et al. (1985), Tollner et al. (1989), Tollner and Verma (1989), Anderson et al. (1988), Warner et al. (1989), and Phogat et al. (1991). These studies and others have looked at the potential of tomography in soil physics, empirically measured machine accuracy, and more recently, have started to apply the technology.

The research presented here was motivated by a unique opportunity. A large, real time weather station network is currently being constructed in Oklahoma (Elliott et al., 1994). The network, Mesonet, is a joint project of Oklahoma State University and the University of Oklahoma, and includes cooperative agreements with several Federal agencies. It will consist of a minimum of 108 stations spread throughout the state, with at least one station

[1]This research was funded in part by a grant from the U.S. Geologic Survey.

 Tomography of Soil-Water-Root Processes. SSSA Special Publication no. 36.

in each of the 77 counties. It will be used for a wide range of research, education, agricultural and emergency planning applications.

As a cooperative contribution, the Oklahoma State Office of the U.S. Soil Conservation Service has agreed to sample and describe the soil at each site. When conditions permit, the soil will be sampled with 50.8-mm hydraulically driven cores. Those cores represent a unique sample set since they will cover a wide range of soils that have been consistently sampled and described. Several properties will also be measured by other researchers. We set out here to determine if the cores could yield any information on the density distribution within the soils and the occurrence of macropores. While we were sure that we could scan the samples, we were less certain that the data would yield any useful information. Our chief concerns were the small sample size and sample disturbance.

This research is a limited program to quantify the value of the cores. Specifically, our objective is to measure dry bulk density distributions on a single soil that was collected by three different methods, analyze the results and determine if the Mesonet cores will be suitable for a larger study. As a result we have also determined the characteristics of the density distribution of the soil tested.

THEORY

The accuracy and precision of tomography methods must be taken into account before measurements are interpreted. It is one thing to see a hole in an image, and another matter to know the accuracy of the hole's diameter and the probability that a smaller hole is present, but not detected. We briefly define here theoretical aspects that apply to these measurements. To generate an image we must measure the attenuation of beams of photons on many paths through a sample. There exists a relationship between the intensity of incident photons, I_0 on the source side of the target with that on the detector side, $I(r,\varphi)$ where r is the ray position and φ is the projection angle. This relationship is the line integral of the function $\mu(x,y)$, the pixel linear attenuation coefficients, along the beam path of diameter w and length L. The attenuation coefficient of each pixel is directly related to the density and material within the pixel area (Gardner, 1986). The attenuation of the beam with initial intensity $I(r,\varphi)$ is given by,

$$In(I_0/I(r,\varphi)) = p(r,\varphi) = \Sigma\, \mu(x,y) \qquad [1]$$

where p is the projection line integral. The convolution back-projection algorithm of Shepp and Logan (1974) is used here to obtain the attenuation image. It is given by,

$$\mu(x,y) = \Delta\varphi\tau \sum_{m=0}^{M} \sum_{n=0}^{N} p(n\tau, \Delta\varphi)\gamma(x \cos m\Delta\varphi + y \sin m\Delta\varphi - n\tau) \qquad [2]$$

where τ is the distance between rays, M is the number of projections, N is the number of rays, $\Delta\varphi$ is the angular step between projections, m and n are summation counters, and γ is a filter function. Note that the constructed image pixel size is independent of the data collection density. The math requires an interpolation, and one to one correspondence is common but not necessary. A pixel attenuation value is thus a weighted average of all ray counts passing through and near the pixel.

A major source of error in CT systems is photon statistics, arising from the random nature of both gamma and x-rays. If we assume that the true value of I_0 is known, Kak and Slaney (1988) showed that the variance image of a reconstruction is given by,

$$s^2\{\mu(x,y)\} = \Delta\varphi\tau \sum_{m=0}^{M} \sum_{n=0}^{N} \frac{\gamma(x\cos m\Delta\varphi + y\sin m\Delta\varphi - n\tau)}{I^*(n\tau, m\Delta\varphi)} \qquad [3]$$

where s^2 is the variance and I^* is the mean value of I. If we use I as an estimate of I^*, Eq. [3] allows the computation of a photon variance image corresponding to the object image. The individual pixel value of that image provides the variance of the corresponding pixel in the object image.

MATERIALS AND METHODS

Instrumentation

The custom pencil-beam gamma ray scanner of Brown et al. (1993) was used in this study. It is similar to machines developed by Crestana et al. (1986), Hainesworth and Aylmore (1983), and others. In this study we used 61 by 61 scanning density for 25.4- and 50.8-mm cores and 121 by 121 scanning density for 100-mm samples. The distance between rays was ≈ 1 mm. Total live count time was either 3 or 10 s. The shortest scan took 4 h, while the longest took 44 h.

Brown et al. (1993) presented a theoretical analysis of this system's accuracy. They showed that CT resolution is a function of the feature size and density, the reconstruction algorithm and the scanning parameters. For the conditions used here, features >1.7 mm will be accurately imaged in both attenuation and size, except for photon statistic errors. Smaller features will be expressed, but their size will be that of a single pixel with an attenuation in between the mean and their true value. We thus consider the system's precision to be 1.7 mm cubed or 5 mm^3.

Computed linear attenuation values were converted to dry bulk density with a calibration. Luo and Wells (1992) have shown that mass attenuation coefficients are insensitive to mineral composition for the high energy, 662 kev gamma rays used here. This results since the photoelectric effect is negligible and compton scattering predominates. They showed that for nine very different soils the theoretical mass attenuation coefficient varied only 1%.

That variation is much less than the variation in packing we would expect from soil standards. Thus, we calibrated the system with a mineral standard of known density, a large quartz crystal. The measured quartz mass attenuation coefficient of the system is 7.52 $m^2 Mg^{-1}$. That value is 3% less than the theoretical value. We attribute the difference to the non-ideal collimation of this real system. Crestana et al. (1986) showed that at lower photon energies, such as the 60 kev gammas given by ^{241}Am, the photoelectric effect plays an important role and gives meaningful contribution to the mass attenuation coefficient. In that case the soil mass attenuation coefficient is strongly dependent on the composition of the soil.

Soil

The soil used in this study was Norge Loam, lying on a 1% slope. The collection site was in Stillwater, OK, with a permanent Bermudagrass [*Cynedon dactylon* (L.) Pers] cover. Its grain size distribution is ≈35% sand, 50% silt, and 15% clay. All samples were collected within 3 m of one another. Hydraulically driven core samples, 25.4 and 50.8 mm in diam., were collected by the U.S. Soil Conservation Service, Oklahoma State Office, as a service to the Mesonet Project. We later collected three hand dug samples, nominally 100 mm in diam. The three sampling methods provide a means to quantify the effects of the sampling method. Samples were carefully transported to the lab, mounted with wax, and vacuum dried at 50 °C. That drying method prevented desiccation cracks from forming in the driven cores, but may not have been successful in preventing their formation in the larger samples.

All scanning was performed at sample depths of 100 to 150 mm. Visual examination of the samples at that depth revealed a generally uniform, homogeneous soil, with a small number of roots. The roots varied from 0.2 to 0.5 mm in diam. One empty root case, 1 mm in diam., was observed. All of those features would be smaller than the system resolution. Thus they will appear in the images as low density pixels, not holes.

Scanning and Image Analysis

The 25.4-mm core was scanned on four progressively deeper planes, each below the previous. They were separated vertically by 2 mm. Ray counts were for 3 s live times. They are identified as Planes C241 through C244. The 50.8-mm core was scanned on 10 planes, 1 through 10. Again, the ray counts were for 3 s and the vertical spacing was 2 mm between planes. Plane 1 was later reimaged with a 10 s live time. That image is noted as 1a. Finally the 100-mm cores were scanned with 10 s live times. Since all 100-mm images were similar, only one image was used for analysis here.

Images were reconstructed with the use of Eq. [2] and displayed for visual inspection with custom software. The raw images show the sample, mounting wax, and background noise. The largest circular area of the samples was visually defined. The pixel values of only that area were used to compute

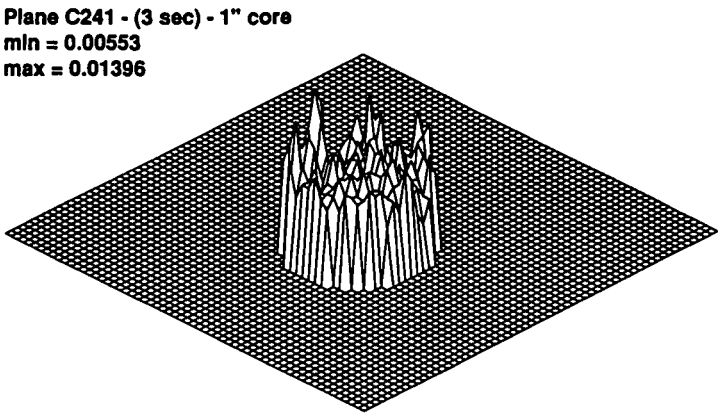

Fig. 7-1. Reconstructed density image for Plane C241.

statistical properties of the distribution. The use of a visual method to define object boundaries introduces human bias, but no better method is currently available.

Once the sample pixels were defined, distribution statistics were determined. Mean, standard deviation, skew and kurtosis were computed by standard methods (Haan, 1979), while the maximum and minimum were determined by inspection. Cross sections through the cores were plotted, and the variance images given by Eq. [3] were determined.

RESULTS AND DISCUSSION

Figures 7-1 and 7-2 present typical images of the attenuation. Figure 7-1 is from the C241 plane of the 25.4 core, while Fig. 7-2 is from the

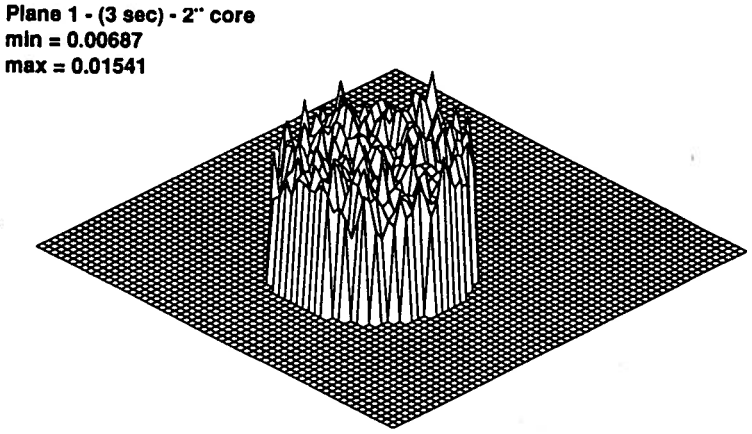

Fig. 7-2. Reconstructed density image for Plane 1.

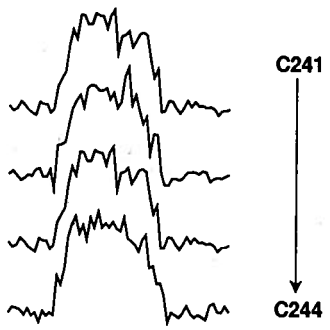

Fig. 7-3. Center line cross sections for 25.4-mm core.

50.8-mm core. In the figures the attenuation is plotted in the vertical direction, and the plane cross sections are plotted above each other to aid comparison. The scale is variable in these plots, but the minimum and maximum is shown for each. None of the cores show macropores. In Fig. 7-1 the 25.4-mm core appears quite variable. This variability is also apparent in Fig. 7-3, which plots cross sections from each of the core planes. The sample is obviously greatly disturbed. Because of this disturbance analysis of the pixel distribution is considered trivial and was not performed.

Figure 7-4 presents cross sections for each plane in the 50.8-mm core. The sloping sides with a slight lip are the wax mounting. These sections show relatively uniform distributions indicating less sample disturbance Plane 1 is the most uniform, while Plane 5 is the most variable. While not apparent in the figure, Plane 5 has a large low density region. Figure 7-5 compares Planes 1 and 1a. Again Plane 1a is the same plane as Plane 1 except it was scanned for 10 seconds per ray. The two images, while having minor differences, are comparable.

Figure 7-6 shows the variance image for the linear attenuation for Plane 1a. The images for the other planes are similar in shape, but higher in value. As can be seen the variance is largest in the center of the sample.

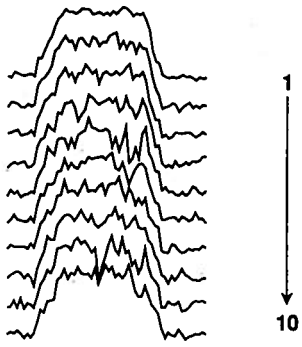

Fig. 7-4. Center line cross sections for 50.8-mm core.

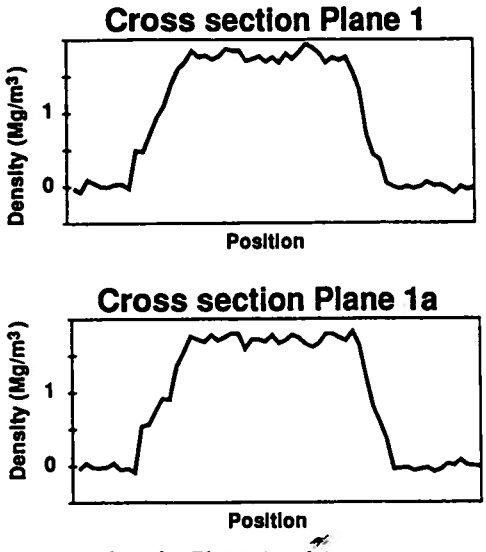

Fig. 7-5. Center line cross sections for Planes 1 and 1a.

Once the soil sample was defined, the density was calculated and the density distribution was computed. Figures 7-7, 7-8, and 7-9 show the cumulative frequency distributions for the previous three planes. Table 7-1 presents the results for each plane. All planes showed negative skew, which would indicate a distribution with a mode greater than the mean. Likewise

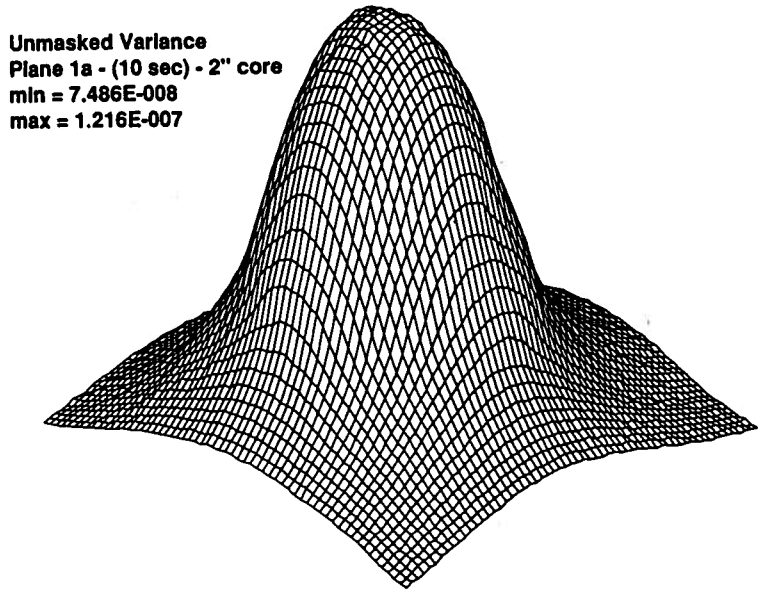

Fig. 7-6. Variance image of Plane 1a.

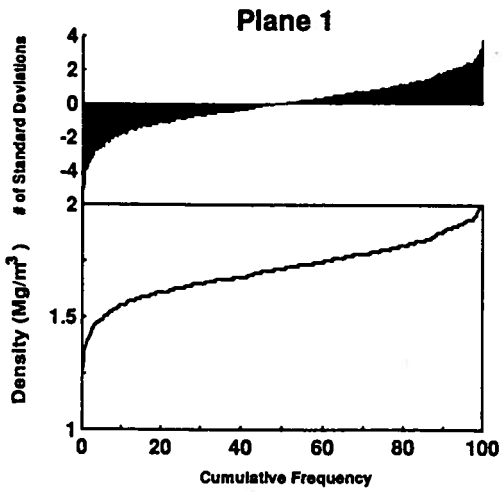

Fig. 7-7. Density distribution for Plane 1.

all planes showed kurtosis less than three indicating a distribution flatter than normal. Planes 5 and 6 have small minimums that are believed to be caused by root casts <1.7 mm. Both planes also have large maximums. While it is possible that these were caused by small rocks we believe that the more likely explanation is that they are caused by the impulse response to the voids, resulting from the use of the filter function (Brown et al., 1993). As such they are artifacts.

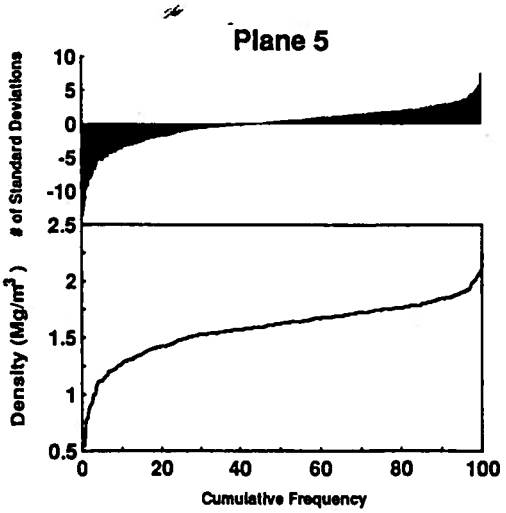

Fig. 7-8. Density distribution for Plane 5.

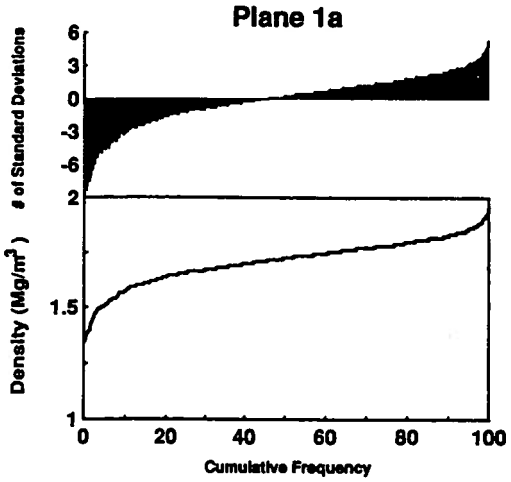

Fig. 7-9. Density distribution for Plane 1a.

Figure 7-10 presents a plot of mean density and density standard deviation. There appears to be an inverse trend between the two, a fairly reasonable relation. Also shown on Fig. 7-7, 7-8, and 7-9 is a measure of the confidence of the pixel values. We have calculated the numbers of photon statistic standard deviations each pixel is from the mean density using the variance images. A large fraction of the pixels are within two photon standard deviations of the mean. Thus we can say little about the true density of those pixels. They could all have the mean value and we would not be able to tell. That is not the case for the pixels at either end of the distributions. They are up to 11 photon standard deviations from the mean and are certainly different from the mean.

Table 7-1. Density statistics for 50.8-mm core.

Plane	Mean	Standard deviation	Skew	Kurtosis	Minimum	Maximum
	Mg m^{-3}				Mg m^{-3}	
1	1.71	0.130	--	--	1.27	2.05
2	1.71	0.129	−0.472	0.695	1.19	2.11
3	1.64	0.175	−0.786	2.286	0.68	2.11
4	1.61	0.222	−7.98	0.911	0.78	2.17
5	1.59	0.250	−1.235	2.929	0.40	2.24
6	1.60	0.207	−0.537	1.012	0.76	2.78
7	1.63	0.199	−0.66	1.289	0.76	2.15
8	1.61	0.203	−0.417	0.435	0.92	2.15
9	1.60	0.196	−0.573	1.416	0.87	2.17
10	1.61	0.182	−0.674	1.463	0.86	2.09
1a	1.71	0.104	−0.754	0.83	1.35	1.96

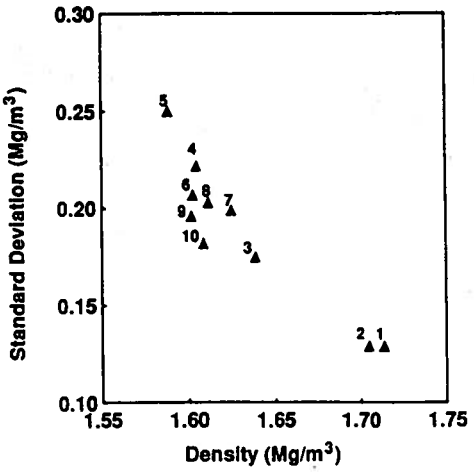

Fig. 7-10. Density variation for 50.8-mm core.

Finally, Fig. 7-11 shows three cross sections for the 100-mm sample. That sample shows several voids. While not visible on the surface we believe those to be desiccation cracks. If so they would not be representative of the native soil. In between the cracks are large areas of solid soil. The density distributions in three areas were calculated. They had means of 1.65, 1.64, and 1.56, while their density standard deviations were 0.177, 0.184, and 0.201. This is consistent with the 50.8-mm core. As such it would indicate that the core was relatively undisturbed.

CONCLUSIONS

The 50.8-mm cores are adequate to discribe the soil density distribution. Thus the Mesonet samples should provide useful information. Because of the low number of small voids in these samples, none were considered adequate to describe the soil macropores. The mean density distribution was

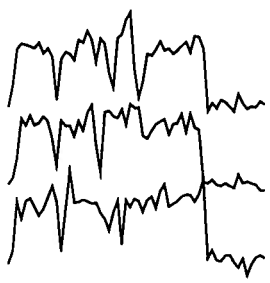

Fig. 7-11. Cross sections of 100-mm sample.

found to vary over small vertical distances. All samples had density distributions with negative skew and kurtosis less than three. The density standard deviation and kurtosis were found to increase with increasing numbers of macropores.

REFERENCES

Anderson, S.H., C.J. Gantzer, J.M. Boone, and R.J. Tully. 1988. Rapid nondestructive bulk density and soil-water content determination by computed tomography. Soil Sci. Soc. Am. J. 52:35–40.

Brown, G.O., M.L. Stone, and J.E. Gazin. 1993. Accuracy of gamma ray computerized tomography in porous media. Water Resour. Res. 29:479–486.

Crestana, S., S. Mascarenhas, and R.S. Pozzi-Mucelli. 1985. Static and dynamic three-dimensional studies of water in soil using computed tomographic scanning. Soil Sci. 140:326–332.

Crestana, S., S. Mascarenhas, and R.S. Pozzi-Mucelli. 1986. Using a computed miniscanner is soil science. Soil Sci. 142:52–61.

Elliot, R.L., F.V. Brock, M.L. Stone, and S.L. Harp. 1994. Configuration decisions for an automated weather station network. Appl. Eng. Agric. 10:45–51.

Gardner, W. 1986. Water content. p. 493–544. *In* A.Klute (ed.) Methods of soil analysis. Part 1. 2 ed. Agron. Monogr. 9. ASA and SSSA, Madison, WI.

Haan, C.T. 1977. Statistical methods in hydrology. Iowa State Univ. Press, Ames.

Hainsworth, J.M., and L.A.G. Aylmore. 1983. The use of computer-assisted tomography to determine spatial distribution of soil water content. Aust. J. Soil Res. 21:435–443.

Kak, A.C., and M. Slaney. 1988. Principles of computerized tomographic imaging. IEEE Press, New York.

Luo, X., and L.G. Wells. 1992. Evaluation of gamma ray attenuation for measuring soil bulk density: 1. Laboratory investigation. Trans. ASAE. 35:17–32.

Petrovic, A.M., J.E. Siebert, and P.E. Rieke. 1982. Soil bulk density analysis in three dimensions by computed tomographic scanning. Soil Sci. Soc. Am. J. 46:445–450.

Phogat, V.K., L.A.G. Aylmore, and R.D. Schuller. 1991. Simultaneous measurement of the spatial distribution of soil water content and bulk density. Soil Sci. Soc. Am. J. 55:908–915.

Shepp, L.A., and B.F. Logan. 1974. The fourier reconstruction of a head section. IEEE Trans. Nucl. Sci. 21:21–43.

Tollner, E.W., J.W. Davis, and B.P. Verna. 1989. Managing errors with x-ray computed tomography when measuring physical properties. Trans. ASAE 32:1090–1096.

Tollner, E.W., and B.P. Verma. 1989. X-ray CT of quantifying water content at points within a soil body. Trans. ASAE 32:901–905.

Warner, G.S., J.L. Nieber, D.D. Moore, and R.A. Geise. 1989. Characterizing macropores in soil by computed tomography. Soil Sci. Soc. Am. J. 53:653–660.